A low-wavenumber analysis of the relative roles of the environmental and vortex-scale variables responsible for rapid intensity changes in landfalling tropical cyclones

Saiprasanth, B.[a], Z. S. Haddad[b], S. Hristova-Veleva[b], and F. D. Marks Jr.[c]

[a]Purdue University, West Lafayette, IN, USA
[b]Jet Propulsion Lab., California Institute of Technology., Pasadena, CA, USA
[c]NOAA/AOML/Hurricane Research Division, Miami, FL, USA

ABSTRACT

Forecasting rapid intensity changes in tropical cyclones (TCs) is hard as the factors responsible span many scales. External and internal dynamical and thermodynamical variables act simultaneously in a nonlinear fashion, either complementing, amplifying, inhibiting or not impacting the TC intensity at all. We try to address the following question: What is the relative importance of the external and vortex-scale variables that influence rapid intensity changes within a TC? Further, which of these variables must be prioritized from an observational standpoint? To answer these questions, a systematic analysis was conducted on a large number of representative TCs to make statistically significant conclusions using discriminant analyses of wavenumber (WN) -filtered fields, with a principal component analysis to detect over-fitting and identify the subset of variables (from the environment and the vortex) consistently correlated with rapid intensity change. Our analyses indicate that a small number of variables wield the most influence on TC rapid intensity changes. The most important variables within the vortex are the WN 0 of precipitation within the radius of maximum winds, the amplitudes of WN 1 of precipitation and the mid-level horizontal moisture flux convergence in the rain band region. Likewise, the most important environmental variables are the angle of the driest air from the shear vector and the magnitude of environmental wind shear. These variables must be prioritized in future observational and consequent data assimilation efforts.

Keywords: Tropical Cyclone, Rapid Intensification, Rapid weakening, Symmetric and asymmetric convection, Bay of Bengal, Linear Discriminant Analysis.

1. INTRODUCTION

Tropical cyclones (TCs) are the product of complex multi-scale processes and nonlinear interactions. The multi-scale processes that influence a TC's intensity occur may be broadly classified as those intrinsic to the vortex and those external to it. The external processes are associated with much larger spatial and temporal scales and therefore, their roles in influencing a TC's intensity are better understood.[1] The intrinsic processes, however are more difficult to observe or predict due to the stochastic nature of convection.[2] However, there exists no objective methodology to quantify the relative importance of those variables within a TC vortex and those external to it in influencing a TC's intensity.[3] In addition to the inherent nonlinearity and stochasticity associated with the processes, there are several uncertainties associated with the numerical modeling of a TC. These uncertainties primarily range from our uncertainty in the knowledge of the model's initial conditions[4] and the representation of the grid-scale and sub-grid scale processes.[5] Therefore, it is very important to understand how any variability associated with the factors influencing a TC's intensity change may be magnified. These problems start to magnify when a TC experiences rapid changes in its intensity (an intensity change of $\pm$ 30 knots or greater in a span of 24 hours[6]), and the forecast errors associated with any one of the drivers can magnify and prove to be very costly. Rapid intensity changes (RICs) comprise rapid intensification (RI) and rapid weakening (RW). Statistical indices developed previously[6–11] for the prediction of RI have largely relied on large-scale environmental variables

Further author information: (Send correspondence to Ziad S. Haddad)
E-mail: zsh@jpl.nasa.gov

Remote Sensing and Modeling of the Atmosphere, Oceans, and Interactions VII, edited by Guosheng Liu
Ziad S. Haddad, Proc. of SPIE Vol. 10782, 1078208 · © 2018 SPIE
CCC code: 0277-786X/18/$18 · doi: 10.1117/12.2500290

due to their persistence and by extension, predictive power. However, recent research has shown that convective-scale processes in the hurricane core might also play a crucial role in influencing rapid changes in TC intensity and structure.[2,12–16] For example, Hendricks et al.[2] concluded that models solely relying on environmental predictors may never be able to capture the RI. Judt et al.[17] postulated that while the environment might largely be responsible for whether a TC undergoes RI or not, the intrinsic processes govern the timing of RI. However, the processes intrinsic to a TC vortex occur at a multitude of spatial and temporal scales and many of the stochastic processes may not be persistent enough to influence a systemic change within the vortex. An inclusion of all such processes may or may not offer any advantage in our ability to predict a critical transition at a vortex-scale. Therefore, it is critical that we identify and include the processes at those scales that have the most persistent and significant impact at a vortex-scale. Additionally, it is important to understand how the processes at other scales impact the evolution of processes at scales that have the most significant impact at a vortex-scale.[18]

Our objective in this study is to develop an empirical framework that can quantify the relative importance of the external and internal vortex-scale variables towards influencing rapid intensity changes in TCs. We hypothesize that a small number of variables wield the largest influence on a TC's intensity change. This is very important from an observational standpoint since this will imply that some variables must be prioritized over the others. Our aim is here to identify those variables in an objective manner and understand how any uncertainty associated with these variables may be magnified over the course of simulation in a forecast model. To achieve this objective, we present an empirical framework that first examines the probability distributions of a set of external and internal variables for TCs that rapidly intensify and weaken; and then objectively identifies the variables that are statistically significant in their difference during time periods that just precede a rapid intensification as opposed to a rapid weakening. The framework then ranks the variables based on how their associated variability will be magnified over the course of model forecasts and how significantly they influence a rapid intensity change in a TC. We also detail the current observations that are available for the variables that are identified as important. We also enlist the gaps in our current observations that limit their utility. The approach and its outcomes are tested for TCs over the Bay of Bengal.

2. DATA AND METHODS

TCs over the Bay of Bengal basin that experienced a rapid intensity change at least once over their life-cycles between 2012-2017 are selected (Table 1). The TCs are not further classified based on their intensity, magnitude of shear, or proximity from land at the time of consideration. A total of 319 cases (158 RI and 151 RW) are obtained from these storms. The assumption here is that the selected cases are representative of the spectrum of TC behavior in the Bay of Bengal. The Weather Research and Forecasting model (WRF, version 3.4.1) is used to simulate the above-mentioned TCs of interest and the details of the model configurations are available in Table 2. These simulation use nested grids in which the resolution of the inner domain is 4km and one-hourly outputs are recorded. The simulations are then transformed to a storm-centric, cylindrical coordinate system where the center is defined as the minimum surface pressure centroid for each time.

2.1 Dimensionality reduction

From the WRF model outputs, the following variables and combinations of thereof are initially selected to describe the instantaneous state of the vortex and the environment just before a rapid intensity change:

- Precipitation
- Radial and vertical component of wind
- Divergence of horizontal wind
- Relative humidity
- Environmental wind shear
- Horizontal moisture flux convergence

Note that this itself would amount to some 10^9 atmospheric state variables in the radial, azimuthal, and vertical dimensions over the domain. To reduce the dimensionality, these variables are first reduced to their wavenumbers (WN) 0 and 1 azimuthal harmonics (the lowest-order symmetric component, WN 0 and the lowest-order asymmetric component, WN 1) using the following equations:[19]

$$f(r,\theta) \approx \hat{f}_0(r) + \hat{a}_1(r)cos(\theta) + \hat{b}_1(r)sin(\theta) \tag{1}$$

$$where \quad \hat{f}_0(r) = \frac{1}{2\pi}\int_{-\pi}^{\pi} f(r,\theta)d\theta, \tag{2}$$

$$\hat{a}_1(r) = \frac{1}{2\pi}\int_{-\pi}^{\pi} f(r,\theta)cos(\theta)d\theta, \tag{3}$$

$$\hat{b}_1(r) = \frac{1}{2\pi}\int_{-\pi}^{\pi} f(r,\theta)sin(\theta)d\theta \tag{4}$$

where $f(r,\theta)$ represents any 2D variable in a storm-centric, cylindrical coordinate framework; r and θ are the independent variables: radius and azimuthal angle respectively; The hats indicate an azimuthal Fourier harmonic and the subscript indicates which harmonic. The assumption made here is that WN 1 represents most of the variance contained in the asymmetries. Since the treatment of our problem of interest is that of an initial value problem, only the initial state (and the boundary conditions) has any effect on the simulated TCs.

The low wavenumber reconstruction (WN 0+1) of 10m tangential winds (intensity) of the individual cases was used to identify the radii corresponding to the maximum winds (RMW), the end of the vortex, and the environmental annulus.

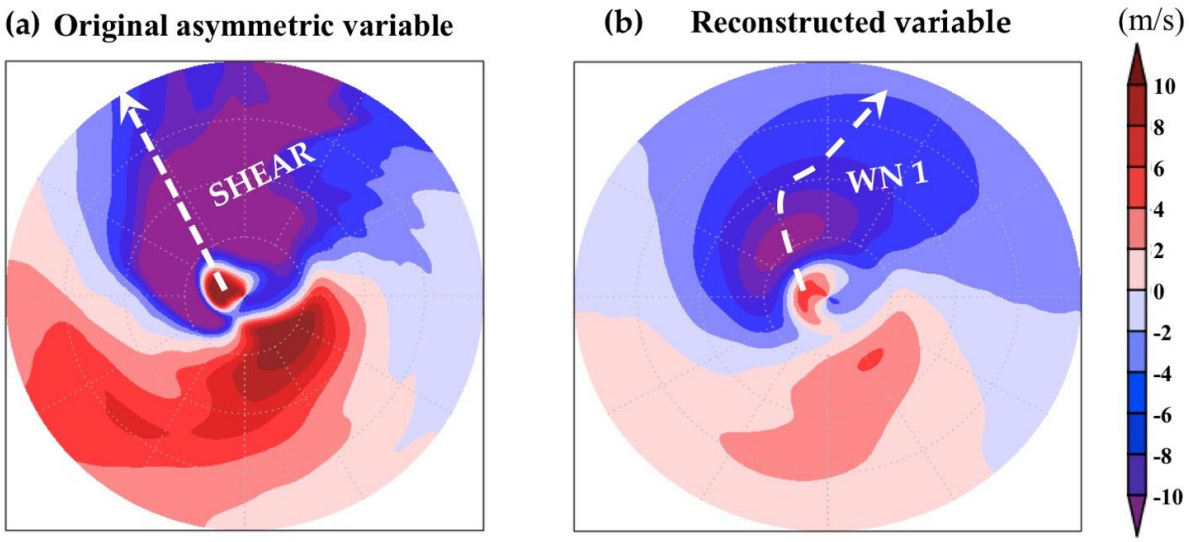

Figure 1. (a) Horizontal cross-section of TC Phailin's radial wind averaged between surface and 850 mb represented in storm-centric, cylindrical coordinates. (b) Same as (a) except that the asymmetric variable is reduced to its lowest wavenumbers. The shear vector and the phase vector of WN 1 are highlighted.

An example of how an original asymmetric variable (low-level radial wind) is reduced to its low wavenumber counterpart is depicted in figures 1 a,b. Also highlighted are the shear (defined as the vector difference between 200 mb and 850 mb averaged winds) vector in the original asymmetric variable and the WN 1 phase vector in the reconstructed variable. The outer boundary of the vortex is defined as the radius at which the WN 0+1 of intensity drops below 8 m/s. The environmental annulus is then defined as the annulus ± 50 km from the radius that marks the end of the vortex. Additionally, the radii between the 2*RMW and 5*RMW is denoted

as the rainband region. Once these regions are defined for each case, the wavenumber 0 and 1 coefficients of the variables enlisted above were obtained and then averaged over a handful of horizontal sectors (the disk within the RMW, the rainband annulus, and the environmental annulus) and four vertical layers (between 1000 - 850 mb, 850 - 700 mb, 700 - 500 mb, and 350 - 200 mb). The initial list of 26 variables that were retained as candidate variables is provided in Table 3.

2.2 Linear Discriminant Analysis

Given that we characterize an initial TC state with a small discrete set of variables $x_1, x_2, \cdots x_n$, the problem of separating points that were characterized as RI from points that are characterized as RW becomes one of finding a hyperplane that separates the two sets of points in n-dimensional space. For two such objectively separated populations (RI and RW) with means $\vec{\mu_{RI}}$ and $\vec{\mu_{RW}}$, and with covariances C_{RI} and C_{RW}, the separation threshold (S) between the two distributions is defined as the ratio of the variances between the two populations to the variance within the populations.[20] The linear discriminant is given by:

$$\alpha_1\sigma_1(\frac{\vec{x_1}}{\sigma_1}) + \alpha_2\sigma_2(\frac{\vec{x_2}}{\sigma_2}) + \cdots + \alpha_n\sigma_n(\frac{\vec{x_n}}{\sigma_n}) \gtrless S \tag{5}$$

where the $\sigma_1 \cdots \sigma_n$ represents the standard deviation of the individual variables $1 \cdots n$ within the population. The $\alpha_1\sigma_1 \cdots \alpha_n\sigma_n$ are the coefficients (weights) associated with each of the normalized variables that may be compared. The variables associated with the biggest normalized weights in the linear discriminant analysis (LDA) are the most significant in causing the separation between the two populations.

To detect over-fitting and identify the subset of variables (from the environment and the vortex) consistently correlated with rapid intensity change, a principal component (PC) analysis of the discriminants is used. Given that we have a repeatable experiment, i.e. training on a reference database to produce a discriminant, we determine how different the outcomes of the experiment are as the reference database is changed. To understand the variability of the discriminants, the coefficients of the discriminant analyses from the multiple data subsets that projected onto the extreme ends of the PC1 versus PC2 space were analyzed. The PC analysis revealed a core subset of variables whose coefficients were essentially constant regardless of the randomized training set used. The core subset of variables identified are:

- 350 - 200 mb (upper-level) horizontal wind divergence (environment)
- WN 0 of rain (within RMW)
- Angle of the driest air from the direction of shear (environment)
- WN 0 of 1000 - 850 mb horizontal moisture flux convergence (within RMW)
- WN 1 of 850 - 700 mb horizontal moisture flux convergence (rain band region)
- Magnitude of environmental vertical wind shear
- Phase overlap between WN 1 of inflow, vertical velocity, and RH within the boundary layer (vortex)
- WN 1 of rain (rain band region)
- Angle of WN1 of rain in the rain bands from the shear direction (vortex)

In this manner, we allowed the LDA to guide the set of variables to be used for analysis without making a subjective assumption regarding the relative importance of these variables. In the following section, only the LDA of the core subset of variables is presented. The discriminants from the each of the randomized training subsets were then averaged to produce a single 'mean' discriminant. This mean discriminant was applied using different values for the critical threshold (S), and the probability of correct diagnosis of RI (pr (estimated RI | true RI) versus the probability of incorrect diagnosis of RI (pr (estimated RI | true RW) were calculated for each threshold. The optimal threshold S, corresponding to (pr (estimated RI | true RI) = 91.07 and (pr (estimated RI | true RW) = 3.97, was identified (see figure 2).

3. RESULTS AND CONCLUSIONS

Figure 2 presents the results of the LDA. The y-axis represents the magnitude of discriminant computed using the left-hand side of Equation 5. The cases that underwent RI in reality, are represented as blue and those that underwent RW in reality, are represented as red. Here, a discriminant higher than the threshold (S) implies that the specific case is estimated by the LDA to undergo RI and a discriminant less than S implies that the case is estimated by the LDA to undergo RW. Thus, the true positives (pr (estimated RI | true RI) in figure 2) and true negatives (pr (estimated RW | true RW) in figure 2) are indicated by blue lines with discriminants over S and red lines with discriminants less than S respectively. Likewise, the false positives (pr (estimated RW | true RI) in figure 2) and false negatives (pr (estimated RI | true RW) in figure 2) are indicated by blue lines with discriminants less than S and red lines with discriminants greater than S. Figure 2 effectively demonstrates that the discriminant computed with a small subset of variables identified by the PCA and LDA can effectively detect RI and RW with a high probability of detection and low probability of false alarm. In other words, as hypothesized earlier, a small number of variables wield the most influence on whether a TC will experience RI or RW.

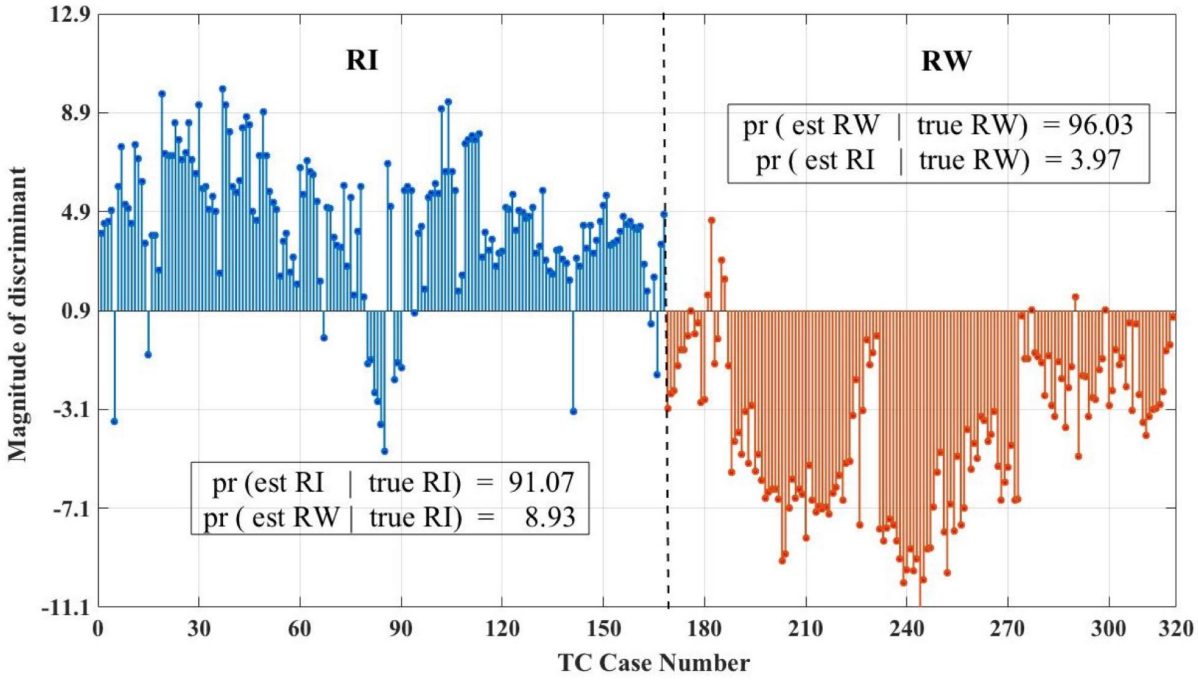

Figure 2. Magnitude of discriminants computed for the RI and RW cases. Also indicated are the probabilities (pr) of true positives, false positives, true negatives and false negatives.

Figure 3 shows the coefficients (weights, w_n) computed using the LDA corresponding to each variable ($w_n = \alpha_n \sigma_n$ as defined in Equation 5). Figure 3 reveals that the most important vortex-scale variables are the amplitudes of the asymmetric fields (WN 1) of 850-700 mb horizontal moisture flux convergence, and WN 1 of rain in the rainband region; and the amplitude of the symmetric field (WN 0) of rain within the RMW. Likewise, the angle between the driest air and the shear vector; and the magnitude of vertical wind shear are the most important environmental variables. The analysis also revealed that the aggregate contribution from the (sum of coefficients of) all the environment variables was comparable to that of all the vortex variables (45:55). In other words, we can conclude that the environment and vortex variables are equally important (with a five percent error) in influencing a rapid intensity change. The role of the weights associated with each of the variables is to magnify the effect of that variable. This means that if there is an uncertainty associated with these variables when they are fed in as inputs into a predictive model, their associated coefficients indicate how the uncertainty in

those variables is magnified. From an observational perspective, this implies that we must know the markers with higher weights much better than the other, by a factor equal to the ratio of their coefficients. Further, the observations of the variables with the highest coefficients must be assimilated as inputs into TC forecasting models for best predictive capabilities.

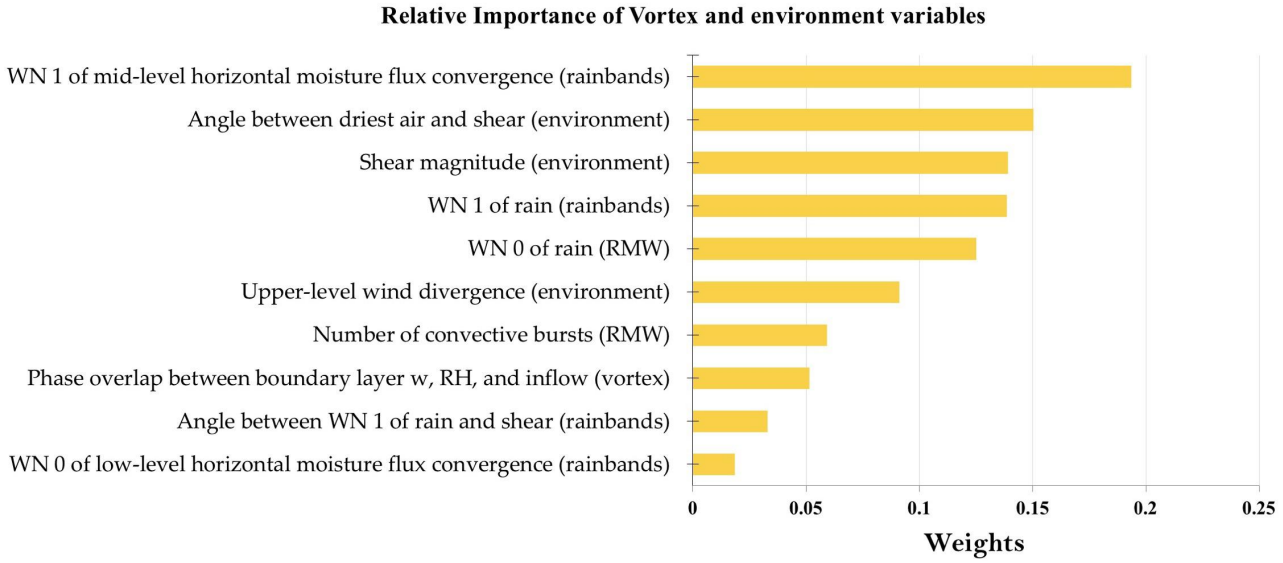

Figure 3. Bar graph showing the weights (results of the LDA) that represent the relative importance of the environment and vortex variables.

4. RELEVANT OBSERVATIONS AND THEIR CURRENT LIMITATIONS

The following section details the kind of observations that may be used to observe the variables that were objectively identified as the most important. In addition, the gaps in our present ability to observe these variables that limit their utility are also detailed.

(a) ***The structure of the 700 - 850 mb horizontal moisture flux convergence in the rain bands***: To estimate this, we need vertically resolved observations of the moisture combined with observations of the flow at different levels. There are satellite observations and estimates of these parameters albeit with limited availability and certainty. The horizontal distribution of moisture in the 700 - 850 mb layer may be obtained from sounder observations such as the Atmospheric Infrared Sounder (AIRS), Microwave Humidity Sounder (MHS), and the Advanced Technology Microwave Sounder (ATMS). However, their estimates are less reliable within the precipitating areas. Since we are interested in the rain band region particularly, observations from Radio Occultation measurements (GNSS-RO) will be very valuable. While their vertical resolution is high, their limitation is the low spatial resolution (150 km) and even more importantly, by their sporadic sampling that does not allow for the retrieval of the 2D structure of moisture. To estimate the flux convergence from observations, one would need observations of the flow field at a given layer. As of today, there are no direct observations of the flow field. However, tracking of features (moisture and/or clouds) has resulted in the development of algorithms to estimate the winds from Geostationary infrared (IR) observations. These Atmospheric Motion Vectors (AMVs) have proven very valuable, in the absence of direct observations. However, caution must be taken while using them as they have uncertainty in the estimates of their altitude. Furthermore, they are absent inside the heavy cloud regions.

(b) ***The amplitude of WN 1 of the precipitation in the rain band region*** - There are a multitude of passive microwave observations from the imagers that are part of the GPM constellation such as Microwave Imager (GMI), Advanced Microwave Scanning Radiometer - 2 (AMSR2), and the Special Sensor Microwave Imager

Sounder (SSMIS). Using the Rain Index - a multi-channel combination of the passive microwave observations developed by Hristova-Veleva et al., (2013),[21] it is possible to easily the precipitating regions, by providing a radar-like depiction and a first-order estimate of the rain intensity. Applying the wave number analysis to the Rain Index allows for a very reliable depiction of the rain bands.

(c) ***The amplitude of WN 0 of precipitation within the radius of maximum winds*** - The precipitation within the RMW region may also be detected using the Rain Index and the Wavenumber analysis. The radius of maximum winds may be detected using surface level scatterometer observations from the Advanced Scatterometer (ASCAT) and RapidScat.

(d) ***The angle between the driest air and the shear vector in the environmental annulus*** - Again, the observations for moisture come from sounders and Radio Occultation measurements as described above. The estimation of shear comes from the atmospheric motion vectors (AMS) described above.

(e) ***The Magnitude of environmental vertical wind shear*** - From the Atmospheric Motion Vectors (AMVs) described above.

In summary, our findings provide guidance-on-guidance for future observational and data assimilation efforts. Furthermore, the framework presented herein may be applied to different ocean basins, with satellite and aircraft observations in addition to model outputs. With this, an empirical forecast of RI and RW that would represent the different environmental conditions (for example, the variability in sea surface temperatures, shear, and water vapor distributions) across the different ocean basins may be developed.

ACKNOWLEDGMENTS

The authors acknowledge WRF data provided by C-DAC Pune and the C-DAC National PARAM Supercomputing Facility. Majority of the work conducted here was performed during S.B's visit to the Jet Propulsion Laboratory, NASA, with financial support in the form of a NASA Earth Science Fellowship (Grant no: NNX15AM72H). The work of Z. S. Haddad and S. Hristova-Veleva was performed at the Jet Propulsion Laboratory, California Institute of Technology, under contract with NASA.

REFERENCES

[1] Emanuel, K., DesAutels, C., Holloway, C., and Korty, R., "Environmental control of tropical cyclone intensity," *Journal of the atmospheric sciences* **61**(7), 843–858 (2004).

[2] Hendricks, E. A., Peng, M. S., Fu, B., and Li, T., "Quantifying environmental control on tropical cyclone intensity change," *Monthly Weather Review* **138**(8), 3243–3271 (2010).

[3] Marks, F. D. and Shay, L. K., "Landfalling tropical cyclones: Forecast problems and associated research opportunities," *Bulletin of the American Meteorological Society* **79**(2), 305–323 (1998).

[4] Emanuel, K. and Zhang, F., "On the predictability and error sources of tropical cyclone intensity forecasts," *Journal of the Atmospheric Sciences* **73**(9), 3739–3747 (2016).

[5] Judt, F., Chen, S. S., and Berner, J., "Predictability of tropical cyclone intensity: scale-dependent forecast error growth in high-resolution stochastic kinetic-energy backscatter ensembles," *Quarterly Journal of the Royal Meteorological Society* **142**(694), 43–57 (2016).

[6] Kotal, S. and Roy Bhowmik, S., "Large-scale characteristics of rapidly intensifying tropical cyclones over the bay of bengal and a rapid intensification (RI) index," *Mausam* **64**(1), 13–24 (2013).

[7] Kaplan, J. and DeMaria, M., "Large-scale characteristics of rapidly intensifying tropical cyclones in the north atlantic basin," *Weather and forecasting* **18**(6), 1093–1108 (2003).

[8] Kaplan, J., DeMaria, M., and Knaff, J. A., "A revised tropical cyclone rapid intensification index for the atlantic and eastern north pacific basins," *Weather and forecasting* **25**(1), 220–241 (2010).

[9] DeMaria, M., DeMaria, R. T., Knaff, J. A., and Molenar, D., "Tropical cyclone lightning and rapid intensity change," *Monthly Weather Review* **140**(6), 1828–1842 (2012).

[10] Kieper, M. E. and Jiang, H., "Predicting tropical cyclone rapid intensification using the 37 ghz ring pattern identified from passive microwave measurements," *Geophysical Research Letters* **39**(13) (2012).

[11] Rozoff, C. M., Velden, C. S., Kaplan, J., Kossin, J. P., and Wimmers, A. J., "Improvements in the probabilistic prediction of tropical cyclone rapid intensification with passive microwave observations," *Weather and Forecasting* **30**(4), 1016–1038 (2015).

[12] Nolan, D. S., Moon, Y., and Stern, D. P., "Tropical cyclone intensification from asymmetric convection: Energetics and efficiency," *Journal of the Atmospheric Sciences* **64**(10), 3377–3405 (2007).

[13] Rogers, R., Reasor, P., and Lorsolo, S., "Airborne doppler observations of the inner-core structural differences between intensifying and steady-state tropical cyclones," *Monthly Weather Review* **141**(9), 2970–2991 (2013).

[14] Chen, H. and Gopalakrishnan, S. G., "A study on the asymmetric rapid intensification of hurricane earl (2010) using the HWRF system," *Journal of the Atmospheric Sciences* **72**(2), 531–550 (2015).

[15] Rogers, R., Zhang, J. A., Zawislak, J., Jiang, H., Alvey III, G. R., Zipser, E. J., and Stevenson, S. N., "Observations of the structure and evolution of hurricane edouard (2014) during intensity change. part ii: Kinematic structure and the distribution of deep convection," *Monthly Weather Review* **144**(9), 3355–3376 (2016).

[16] Leighton, H., Gopalakrishnan, S., Zhang, J. A., Rogers, R. F., Zhang, Z., and Tallapragada, V., "Azimuthal distribution of deep convection, environmental factors, and tropical cyclone rapid intensification: A perspective from HWRF ensemble forecasts of hurricane edouard (2014)," *Journal of the Atmospheric Sciences* **75**(1), 275–295 (2018).

[17] Judt, F. and Chen, S. S., "Predictability and dynamics of tropical cyclone rapid intensification deduced from high-resolution stochastic ensembles," *Monthly Weather Review* **144**(11), 4395–4420 (2016).

[18] Saiprasanth, B., Krishnamurti, T. N., Dubey, S., Shreevastava, A., Chavas, D. R., and Marks Jr, F., "On the role of convective asymmetries during tropical cyclone rapid intensity changes," *Journal of the Atmospheric Sciences* **Manuscript submitted** (2018).

[19] Vukicevic, T., Uhlhorn, E., Reasor, P., and Klotz, B., "A novel multiscale intensity metric for evaluation of tropical cyclone intensity forecasts," *Journal of the Atmospheric Sciences* **71**(4), 1292–1304 (2014).

[20] Fisher, R. A., "The use of multiple measurements in taxonomic problems," *Annals of eugenics* **7**(2), 179–188 (1936).

[21] Hristova-Veleva, S., Callahan, P., Dunbar, R., Stiles, B., Yueh, S., Huddleston, J., Hsiao, S., Neumann, G., Vanhoff, B., Gaston, R., et al., "Revealing the winds under the rain. part i: Passive microwave rain retrievals using a new observation-based parameterization of subsatellite rain variability and intensityalgorithm description," *Journal of Applied Meteorology and Climatology* **52**(12), 2828–2848 (2013).

Tropical Cyclone	Initialization dates and times
Nilam	0 UTC, 28th October 2012; 0 UTC, 29th October 2012; 0 UTC, 30th October 2012.
Viyaru	0 UTC, 12th May 2013; 0 UTC, 13th May 2013; 0 UTC, 14th May 2013;
Phailin	0 UTC, 9th October 2013; 0 UTC, 10th October 2013; 0 UTC, 11th October 2013;
Helen	0 UTC, 20th November 2013; 0 UTC, 21st November 2013; 0 UTC, 22nd November 2013;
Lehar	0 UTC, 26th November 2013; 0 UTC, 27th November 2013; 0 UTC, 28th November 2013;
Madi	0 UTC, 12th December 2013; 0 UTC, 13th December 2013; 0 UTC, 14th December 2013;
Hudhud	0 UTC, 9th October 2014; 0 UTC, 10th October 2014; 0 UTC, 11th October 2014;
Roanu	0 UTC, 18th May 2016; 0 UTC, 19th May 2016; 0 UTC, 20th May 2016;
Kyant	0 UTC, 23rd October 2016; 0 UTC, 24th October 2016; 0 UTC, 25th October 2016;
Nada	0 UTC, 29th November 2016; 0 UTC, 30th November 2016; 0 UTC, 1st December 2016;
Vardah	0 UTC, 11th December 2016; 0 UTC, 12th December 2016; 0 UTC, 13th December 2016;

Table 1. The selected list of tropical cyclones (TCs) over the Bay of Bengal. Also, the dates and times of initialization (cycles) of the TCs in the numerical model are provided. The length of each simulation was 72 hours. In each of the selected cycles, the instances just preceding a rapid change in intensity was obtained, and all the variables are extracted at these times.

Model used	WRF-ARW v3.4.1
Resolution	Two-way Nested domain with 12 km and 4 km resolution (36 vertical levels)
Initialization	NCEP GFS 0.5deg data
Forecast Updates	Daily with 00Z initial condition
Forecast Period	72 hours with hourly interval
Domain size	7.12196 N to 37.3972 N; 63.9995 E to 97.609 E
Cumulus Physics	Kain-Fritsch Scheme
Microphysics	Thompson
Long wave radiation scheme	Rapid Radiative transfer model - G
Short wave radiation scheme	Rapid Radiative transfer model - G
Surface layer physics	Eta similarity scheme
Land surface scheme	Unified NOAH
Boundary layer physics	Yonsei University Scheme

Table 2. Details of the Weather Research and Forecasting model set-up

1	WN0 of Divergence of the wind at 200-300 hPa in the environmental annulus
2	WN0 of rain at the environmental annulus
3	WN0 of rain within the RMW
4	WN0 of rain in the rain band region
5	WN0 of environmental relative humidity at 850-700 hPa
6	WN0 of environmental relative humidity at 1000-850 hPa
7	WN0+1 environmental relative humidity at 850-700 hPa - Averaged in a quadrant around the max asymmetry
8	WN0+1 environmental relative humidity at 1000-850 hPa - Averaged in a quadrant around the max asymmetry
9	WN0+1 environmental relative humidity at 850-700 hPa - Averaged in a quadrant around the min asymmetry
10	WN0+1 environmental relative humidity at 1000-850 hPa - Averaged in a quadrant around the min asymmetry
11	Angle of the driest environmental air from the direction of shear
12	WN0 of the 1000-850 hPa horizontal moisture flux convergence within the RMW
13	WN1 of the 1000-850 hPa horizontal moisture flux convergence within the RMW
14	WN0 of the 850-700 hPa horizontal moisture flux convergence in the rain band region
15	WN1 of the 850-700 hPa horizontal moisture flux convergence in the rain band region
16	WN0 of the 1000-850 hPa radial wind within RMW
17	WN0+1 of the 1000-850 hPa radial wind within the RMW - Averaged in a quadrant around maximum inflow asymmetry
18	WN0 of the 850-700 hPa radial wind within the RMW
19	Magnitude of environmental shear (difference between 850 and 200 hPa)
20	Convective bursts (Number of cells with vertical velocity greater than 1m/s at 8km (350 hPa)) within RMW
21	Phase overlap between boundary layer inflow, maximum of relative humidity, and upward vertical velocity within the vortex
22	Phase overlap between boundary layer inflow, minimum of relative humidity, and downward vertical velocity within the vortex
23	Magnitude of WN1 of rain within the RMW
24	Magnitude of WN1 of rain in the rain bands
25	Angle of WN1 of rain within RMW from shear direction
26	Angle of WN1 of rain in the rain bands from shear direction

Table 3. List of variables after low wavenumber reconstruction